Original Article

A recapitulative three-dimensional model of breast carcinoma requires perfusion for multi-week growth

Journal of Tissue Engineering
Volume 7: 1–15

DOI: 10.1177/2041731416660739
tej.sagepub.com
SAGE

Kayla F Goliwas[1], Lauren E Marshall[2], Evette L Ransaw[1], Joel L Berry[2] and Andra R Frost[1]

Abstract

Breast carcinomas are complex, three-dimensional tissues composed of cancer epithelial cells and stromal components, including fibroblasts and extracellular matrix. In vitro models that more faithfully recapitulate this dimensionality and stromal microenvironment should more accurately elucidate the processes driving carcinogenesis, tumor progression, and therapeutic response. Herein, novel in vitro breast carcinoma surrogates, distinguished by a relevant dimensionality and stromal microenvironment, are described and characterized. A perfusion bioreactor system was used to deliver medium to surrogates containing engineered microchannels and the effects of perfusion, medium composition, and the method of cell incorporation and density of initial cell seeding on the growth and morphology of surrogates were assessed. Perfused surrogates demonstrated significantly greater cell density and proliferation and were more histologically recapitulative of human breast carcinoma than surrogates maintained without perfusion. Although other parameters of the surrogate system, such as medium composition and cell seeding density, affected cell growth, perfusion was the most influential parameter.

Keywords

Breast carcinoma, three-dimensional, perfusion, bioreactor, tumor microenvironment, in vitro models

Received: 5 May 2016; accepted: 26 June 2016

Introduction

Traditionally, preclinical research in the field of cancer biology has involved in vitro analysis of cell behavior, predominately utilizing two-dimensional (2D) cell culture, and in vivo studies using animal models. It is well appreciated that these two types of model systems differ widely, including differences in dimensionality and in the microenvironment surrounding cancer cells.[1–4] Differences between these two models, as well as the inherent differences between these models and human malignancies, may lead to inaccurate assessment of cancer biology. Culture methods that better bridge the gap between in vitro and in vivo models have been developed, including the use of cell spheroids, microfluidics platforms, and solid three-dimensional (3D) culture in an extracellular matrix (ECM), yet many current methods still lack crucial parameters such as *human* stromal cells, relevant ECM, and/or an appropriate volume to best mimic a human tumor in vivo.[5–11] Each of these components (i.e. stromal cells, ECM, and volume/dimensionality) is known to affect cellular behavior and therapeutic response; therefore, it is not surprising that currently utilized in vitro and animal model systems often do not accurately predict the efficacy of candidate therapeutics. This is reflected in the extremely low

[1]Department of Pathology, The University of Alabama at Birmingham, Birmingham, AL, USA
[2]Department of Biomedical Engineering, The University of Alabama at Birmingham, Birmingham, AL, USA

Corresponding author:
Andra R Frost, Department of Pathology, The University of Alabama at Birmingham, 1824 6th Ave. S., WTI 320B, Birmingham, AL 35233, USA.
Email: afrost@uabmc.edu

number of candidate therapies that progress to clinical use. Only 7% of drugs that enter Phase I clinical trials in the field of oncology become useful therapeutics.[12]

The volume or dimensionality associated with human cancers can greatly affect oxygen and nutrient gradients, which, in turn, may result in non-uniform drug exposure and diffusion as well as interstitial pressure and/or blood flow disturbances.[13] The dimensionality of cancers also creates a dynamic 3D architecture that allows malignant cells to take cues from their microenvironment, including matrix proteins and stromal cell populations. These parameters impact therapeutic efficacy and can alter drug response in vivo, yet most current in vitro models have a thickness or maximum diameter of less than 500 µm, with some spheroid models reaching 1–3 mm in dimension.[2,7,13–15] Whereas most breast carcinomas detected by mammography have a diameter of 1.0 cm or greater.[7,15,16]

Tissue engineered 3D in vitro models can be designed to include important components of the tissue microenvironment, such as human stromal cells and ECM, in a more relevant volume.[4,17] Models that include these components are particularly important for studies that aim to evaluate the effect of the tumor microenvironment on malignant cell behavior, as well as the evaluation of therapeutic efficacy. However, the increased dimensionality of these model systems may limit oxygen and nutrient diffusion which could negatively affect viability and growth, especially with multi-day or multi-week culture.

While 3D in vitro tissue models offer many benefits, there is an increased experimental complexity associated with this type of model. The added complexity of dimensionality and the presence of multiple cell types require precise optimization of each experimental parameter to obtain sufficient growth and sustain these models effectively. Herein, the development and characterization of a 3D tissue engineered breast carcinoma surrogate with a more relevant volume, human cell composition, and tumor microenvironment is described. The surrogates are composed of ECM containing MDA-MB-231 breast cancer epithelial cells (ECs) and human cancer-associated fibroblasts (CAFs) within a structural scaffold, with a total surrogate volume of 1.2 cm^3 and maximum dimension of 1.0 cm. To maintain viability, this volume is penetrated by four (400 µm) channels and housed in a bioreactor system (described in detail in Marshall et al.,[18] shown in Figure 1) to deliver nutrients via continuous perfusion using a micro-peristaltic pump. Surrogates were assessed for their ability to recapitulate the morphology and cellularity of human breast carcinoma and for the maintenance of growth over multiple weeks. Each component of the model (i.e. ECM, constitute cells, and medium) was varied and the resulting impact on morphology and cellularity was determined after multi-week growth.

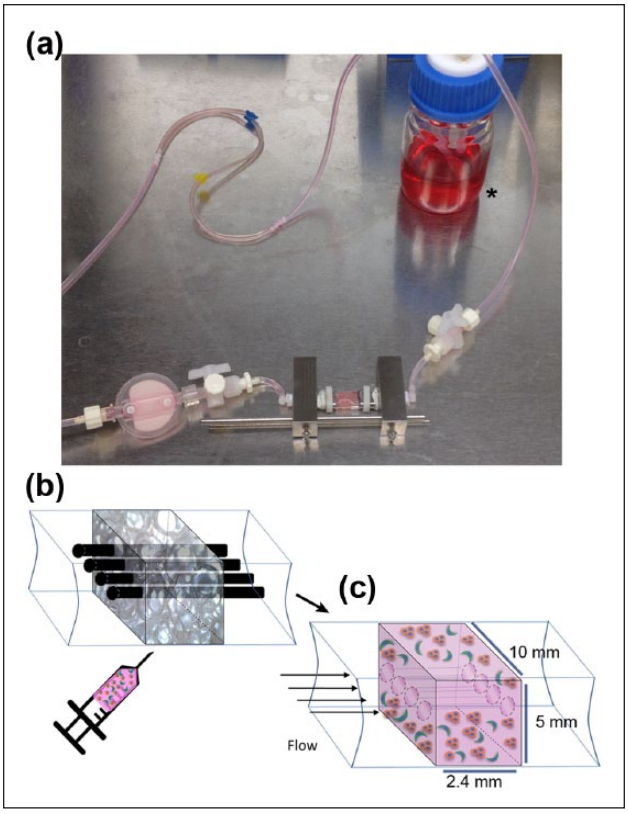

Figure 1. Bioreactor design. (a) Image of the bioreactor system which is constructed from a PDMS flow channel that contains the breast carcinoma surrogate. The bioreactor is connected by tubing to a media reservoir (asterisk) and a micro-peristaltic pump (pump not shown). (b) Cartoon representation of the breast carcinoma surrogate setup. The PDMS flow channel, containing a PDMS foam (gray 3D rectangle) that functions as a structural support and four 400-µm wires (top), gets injected with the cell–ECM mixture. (c) Following ECM polymerization, wires are removed to create four microchannels to allow for delivery of medium to the surrogate following connection to the bioreactor and micro-peristaltic pump (breast cancer epithelial cells (orange) and CAF (green) embedded in ECM (pink), PDMS foam not shown).

Methods

Characterization of hematoxylin and eosin–stained sections of human breast carcinoma

Hematoxylin and eosin (H&E)-stained histologic sections of human breast cancer were obtained from the archives of the University of Alabama at Birmingham (UAB) Department of Pathology after approval from the UAB Institutional Review Board for Human Use. A waiver of patient authorization was requested and subsequently approved by the UAB Institutional Review Board for Human Use. Tumor grade was determined by a trained anatomic pathologist (A.R.F.) using the Nottingham Histologic Score.[19] All tumors evaluated were infiltrating ductal carcinomas (carcinoma of no special type).

The numbers of ECs and fibroblasts were manually counted in photomicrographs of H&E-stained histologic sections (400×), based on morphologic criteria and location in the tissue by two independent reviewers. The ratio of ECs to fibroblasts (E:F), cell density, and cell aggregation were determined by evaluating five representative fields of view (FOVs) for each case, as described below.

Image analysis of histologic sections for cell aggregation, cell density, and percent area occupied by cells

Cell aggregation, cell density, and the percent area occupied by cells were determined on photomicrographs (400×) of H&E-stained histologic sections of human breast carcinoma tissues (five representative photomicrographs of each breast carcinoma analyzed) or surrogates (complete cross sections of each surrogate analyzed). The number of cell aggregates was determined using the ImageJ Colony Blob Count Tool plugin with background subtraction, the application of a Gaussian filter, and a minimum group size of 5000 pixels. The number of aggregates was normalized to the cross-sectional area so that cellular aggregation was defined as the number of cellular aggregates per 1×10^6 pixels^2 (area). The same photomicrographs were used to manually evaluate cell density, which was defined as the number of nucleated cells per 1×10^6 pixels^2 (area). The percent area occupied by cells was determined using the polygon tool in ImageJ where the total portion of the matrix containing cells was divided by the total surrogate area and multiplied by 100, for each surrogate.

Cell culture

MDA-MB-231 cells (231) were obtained from Dr Danny Welch (University of Kansas) and the human mammary microvascular endothelial cells (HMMECs) were obtained from ScienCell. The identity of the 231 cell line was confirmed by STR analysis (DNA profiling performed in the UAB Heflin Genomics Core Laboratory). CAFs were isolated by us as described previously,[20] after approval from the UAB Institutional Review Board for Human Use. A waiver of patient authorization (i.e. informed consent) was requested and subsequently approved by the UAB Institutional Review Board for Human Use. Subsequently, CAF and HMMEC were immortalized via transduction of human telomerase (CAF-hTERT and HMMEC-hTERT) followed by mass selection, verification of hTERT overexpression (data not shown), and continued growth. The MDA-MB-231 cell line was maintained in Dulbecco's modified Eagle's medium (DMEM; Corning) supplemented with 10% fetal bovine serum (FBS; Atlanta Biologicals) (EC complete growth medium). CAF-hTERTs were maintained in DMEM supplemented with 10% FBS and 10 μg/mL hygromycin (MP Biologics). HMMEC-hTERTs were maintained in endothelial basal medium (ScienCell) supplemented with 5% FBS (ScienCell), endothelial cell growth supplement (ScienCell), and 10 μg/mL hygromycin (HMMEC medium). Spheroids were formed by culturing 231 cells on 1% agar-coated 10-cm dishes for 3 days prior to incorporation into 3D cultures.

Surrogate preparation

Solid 3D surrogate preparation. Four concentrations (1.9, 4.0, 6.0, and 8.0 mg/mL) of pepsin-extracted collagen type I (bovine; Advanced Biomatrix) were utilized in combination with 10% (by volume) growth factor reduced Matrigel (BM; BD Biosciences). The 231 cells and CAF-hTERT (2:1) (2.1×10^6 total cells/100 μL ECM) were incorporated into each ECM combination. In all, 100 μL of cell–ECM mixture was plated into each well of an eight-well chamber slide (Thermo Scientific) and the mixture was polymerized for 45 min at 37°C, 5% CO_2. Following ECM polymerization, 100 μL low-serum EC medium (DMEM + 0.05% FBS) was added on top of solid 3D surrogates. Surrogates were maintained for 7, 14, or 21 days with medium changed every 2 days. For solid 3D cultures containing 231 cell spheroids, 1.5×10^6 cells were grown on 1% agar-coated 10-cm dishes. The resulting spheroids and 7×10^5 CAF-hTERT (single-cell suspension) were incorporated per 100 μL ECM, for a cell concentration of approximately 2.2×10^6 total cells/100 μL ECM and an E:F ratio of 2:1. Following culture, surrogates were fixed in buffered formalin and paraffin-embedded (FFPE) for histological analysis.

Non-perfused and perfused 3D surrogate preparation. The 231 cells and CAF-hTERT (2:1 E:F ratio, 2.1×10^6 or 1.05×10^6 total cells/100 μL ECM) were mixed into an ECM containing 6.0 mg/mL bovine collagen I + 10% BM (by volume) and injected into a polydimethylsiloxane (PDMS) foam within the PDMS bioreactor housing/flow channel (Figure 1, PDMS foam measuring approximately 10 mm × 2.4 mm × 5 mm and penetrated by four 400-μm Teflon-coated wires located within the PDMS flow channel). Description of the preparation of the PDMS foam is presented subsequently. Following ECM polymerization, the Teflon wires were removed, generating four microchannels in the ECM–cell mixture and PDMS foam. Non-perfused surrogates in the flow channel were then placed into a bath of 20 mL low-serum EC medium (DMEM + 0.05% FBS) for 7, 14, or 21 days and medium was changed every 7 days. Perfused surrogates in the flow channel were placed in the bioreactor support structure and connected to a micro-peristaltic pump and a media reservoir via silicone tubing, as previously described[18] and depicted in Figure 1, and continuously perfused with 20 mL medium (DMEM + 0.05% FBS or HMMEC media

containing 5% FBS) for 7, 14, or 21 days, with media changed every 7 days. Following growth, surrogates were processed (FFPE) and histological sections were prepared, as previously described.[18]

PDMS foam preparation

Alginate beads were formed by dispensing a 2% sodium alginate solution dropwise into 1% calcium chloride containing 0.5% Tween-20 using a 26- or 31-G needle. Following formation, alginate beads were mixed with PDMS elastomer and curing agent (Sylgard® 184 Silicone Elastomer Kit; Dow Corning; 10:1 ratio) in a 35-mm Petri dish. Vacuum pressure was applied briefly and the mixture was cured overnight at room temperature. Following PDMS curing, alginate beads were dehydrated using vacuum pressure incubation at 60°C. Dehydrated beads were washed from the resulting foam and the foam was sterilized prior to use, as described in Calcagnile et al.[21]

Immunohistochemistry and analysis

Histologic sections of FFPE surrogates were immunostained with anti-Ki-67 (Clone Sp6; Thermo Scientific; 1:100 dilution) or anti-cleaved caspase 3 (Cell Signaling; 1:100 dilution), following heat-induced antigen retrieval using pH 6.2 citrate buffer (Biogenex). Dako Envision + Dual Link System HRP kit, containing the DAB + chromogen was used for secondary detection. The percentage of positively stained nuclei (Ki-67 labeling or cleaved caspase 3 labeling) per FOV was counted, with a minimum of 400 cells analyzed per replicate surrogate.

Quantifying E:F in tumor surrogates

Serial histologic sections (complete cross sections of each surrogate) were immunostained to distinguish 231 cells from CAF-hTERT. Anti-cytokeratin 8 (CK8) (1:150; Thermo Scientific), detected with anti-mouse Alexa 594 (1:500; Life Technologies), was used to stain 231 cells following heat-induced antigen retrieval using citrate buffer (pH 6). Anti-fibroblast activation protein (FAP) (1:200; R&D), detected with anti-sheep Alexa 488 (1:500; Life Technologies), was used to stain CAF-hTERT. 4′,6-Diamidino-2-phenylindole (DAPI) (1:1000) was used as a nuclear counterstain. A minimum of 500 cells were analyzed per replicate surrogate. Marker specificity was verified prior to staining using FFPE histologic sections containing each cell type separately. To evaluate each cell population, the percentage of cells that were FAP-positive and the percentage of cells that were CK8-positive were determined for each surrogate. These values were compared to the original proportion of each cell type incorporated into the surrogates.

Elastic modulus measurement

Using a dynamic mechanical analyzer (DMA; PerkinElmer), cyclic unconfined compression testing was completed on polymerized ECM samples, without cells embedded, in a humidified chamber at 37°C. Compression testing was completed at 1-Hz frequency following 20% preconditioning for 20 cycles. The elastic modulus was calculated using values obtained between 0% and 3% strain.

Growth curve analysis

The 231, CAF-hTERT, and HMMEC-hTERT were grown in standard 2D culture in each of the following media combinations: EC complete growth medium, low-serum EC medium, and HMMEC medium. Growth curves were generated by counting the number of viable cells per well (via trypan blue staining) every 24 h for 8 days. Three replicate wells were evaluated per time point.

Statistics

One-way analysis of variance (ANOVA) with multiple comparison testing was used to evaluate significant differences between three or more groups. Unpaired Student's t-test was used to evaluate significant differences between two groups. Pearson's correlation coefficient was computed to evaluate correlations between two groups.

Results

Endpoint parameters are defined by histologic sections of human breast carcinoma

Breast carcinoma is a heterogeneous disease that often presents histologically as aggregates of breast carcinoma ECs surrounded by stromal cells, predominately CAF, and ECM. The degree of cell aggregation, the number of stromal cells, and the total number of cells per tumor area can vary greatly within this disease. Characterization of these parameters from several cases of human breast carcinoma provided a baseline with which to compare our breast carcinoma surrogates. Because the methods used to evaluate the tissue surrogates are similar to those used in the routine clinical evaluation of human breast carcinomas (i.e. utilization of histologic sections of FFPE tissues), characterization of endpoint parameters of interest in breast carcinoma samples provided the most relevant comparison to ensure accurate histological recapitulation. The number of cells per area (cell density), the degree of cell aggregation, and the E:F were evaluated on five representative photomicrographs of H&E-stained histologic sections for each of the eight breast carcinomas. In tissues, the cancer ECs are cytologically atypical and often show some degree of aggregation, whereas the stromal fibroblasts have round to spindled nuclei and lie singly in abundant ECM. These

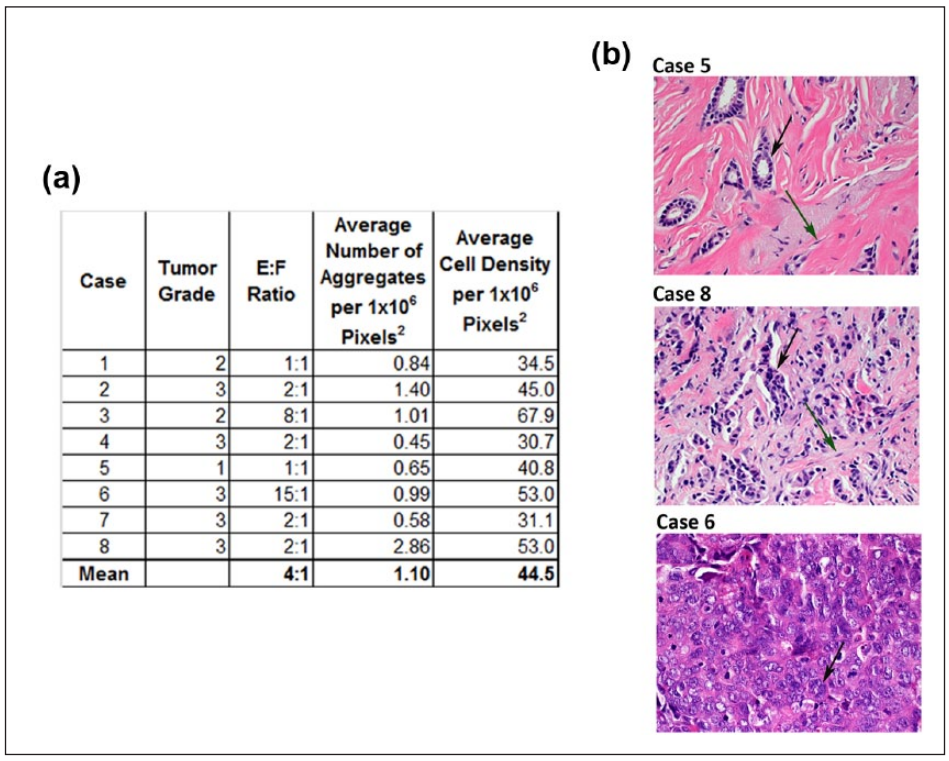

Case	Tumor Grade	E:F Ratio	Average Number of Aggregates per 1x10^6 Pixels^2	Average Cell Density per 1x10^6 Pixels^2
1	2	1:1	0.84	34.5
2	3	2:1	1.40	45.0
3	2	8:1	1.01	67.9
4	3	2:1	0.45	30.7
5	1	1:1	0.65	40.8
6	3	15:1	0.99	53.0
7	3	2:1	0.58	31.1
8	3	2:1	2.86	53.0
Mean		**4:1**	**1.10**	**44.5**

Figure 2. Characterization of H&E-stained histologic sections of human breast carcinoma. (a) Table summarizing the characterization of tumor histologic grade, epithelial-to-stromal-cell ratio (E:F), cell aggregation, and cell density of eight human breast carcinomas. Characterization was completed using image analysis of photomicrographs with an original magnification of 400×. The mean value of parameters is reported in the final row. (b) Photomicrographs (400×) demonstrating the morphologic variability between patients' tumors. Green arrows indicate CAF; black arrows indicate cancer epithelial cells.

morphologic features were used to distinguish and count these two cell types to arrive at an E:F. The Nottingham Histologic Score[19] was used to assign a histologic grade (Figure 2(a)). The degree of variability in the measured parameters between cases reflected the heterogeneity of breast carcinoma. This variability can be appreciated in Figure 2(b), which shows photomicrographs of H&E-stained sections from three cases with distinct E:F, cell aggregation, and cell density. The median E:F found in the eight cases evaluated was 2:1 (range 1:1–15:1), depicted in the middle photomicrograph (case 8) of Figure 2(b). The mean E:F, number of aggregates, and cells per area (1×10^6 pixels^2) are presented in Figure 2.

PDMS foam is a supporting scaffold for use in the bioreactor system

The current design of our bioreactor system utilizes a support structure, or scaffold, to stabilize the tissue surrogates during growth so that they can withstand fluid flow. Previously, we have used a carbon foam to provide the necessary stabilization.[18] While this scaffold provided the support needed, it was not optically clear, making it challenging to evaluate growth during culture. A scaffold that is inert, provides support, is easily sectioned for histology, and has optical clarity would be ideal. A PDMS foam was generated using methods similar to those previously described[21] and was evaluated for use in this system. PDMS is a silicone-based organic polymer that is inert and known to be non-toxic to cells. To make the foam, alginate beads were formed using 26- and 31-G needles, as shown in Figure 3(a) (top panels). The beads were closely packed together and incorporated into the PDMS prior to curing. Following curing, beads were dehydrated and removed from the PDMS to generate a porous foam (Figure 3(a)) with partially interconnecting pores. The pore sizes of the foams produced using beads prepared with 26- and 31-G needles were measured. As expected, significantly larger pores were created in the foam using 26-G beads (Figure 3(b), unpaired t-test, $p \leqslant 0.001$).

The optical clarity of the PDMS foam was evaluated by injecting ECM containing 231 cells into the foam backbone and imaging using brightfield microscopy (Figure 3(c)). The foam did not hinder the visibility of cells. Furthermore, the foam withstood fixation and processing to paraffin and could be easily sectioned with a tissue microtome (Figure 3(d)). The foam made using 26-G beads (average pore diameter of 1.2 mm) was chosen for subsequent use in the bioreactor to provide more area, or larger pores, for cell growth over time.

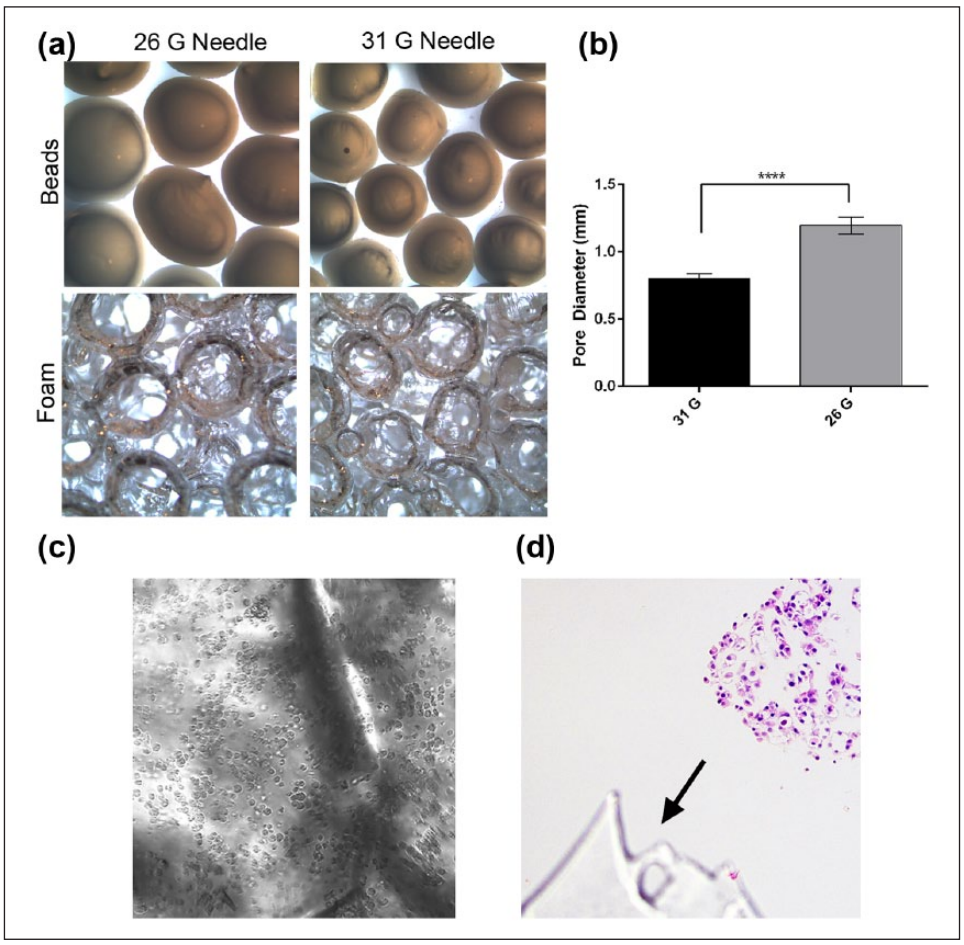

Figure 3. Generation of PDMS foam. (a) Photographs depicting alginate beads (top) and consequent pore size of the PDMS foam (bottom) when 31- and 26-G needles are used to make the beads. (b) Graphical comparison of pore diameter within the foam when 31- and 26-G needles are used to make the alginate beads. Data are the mean and SEM, unpaired t-test, ****$p \leqslant 0.0001$. (c) Photomicrograph of 231 cells and ECM within PDMS foam (brightfield microscopy, 200× original magnification). (d) Photomicrograph of an H&E-stained histologic section of a surrogate showing PDMS on the histologic section (arrow, 200× original magnification).

Elastic modulus of ECM varies with collagen I concentration

The ECM in breast carcinoma is predominately composed of collagen type I with much lower concentrations of other matrix proteins, including those found in basement membrane (BM).[22–25] To reflect this, the ECM utilized here is predominately collagen type I (90%) with the addition of 10% BM (GFR Matrigel). While breast carcinoma often contains increased ECM deposition that is altered in composition from the ECM in normal breast,[26] to our knowledge the concentrations of specific ECM components in human breast cancers have not been directly measured. It is well appreciated that the mechanical characteristics of malignant tissues are dysregulated compared to normal tissues.[27–29] In particular, the stiffness or elastic modulus is increased due to increased matrix deposition and cell rigidity in response to biochemical and biomechanical cues from the microenvironment. The increase in ECM stiffness and cancer cell rigidity activates cell signaling cascades that enhance cancer cell migration and invasion.[27,30,31] The elastic modulus of ECM is affected by the concentration of collagen and other ECM proteins, with increased concentrations correlating with an increase in the elastic modulus of the ECM.[28,32,33] To determine a collagen concentration that approximates the elastic modulus reported for mammary cancers,[29,34] a DMA was used to measure the elastic modulus of ECM composed of 90% collagen I and 10% BM with collagen concentrations of 1.9, 4.0, 6.0, and 8.0 mg/mL. Cyclic unconfined compression testing was completed on polymerized ECM samples. The elastic modulus increased with increasing collagen concentration, as expected (Table 1). The reported values for the elastic moduli of mammary cancers vary widely and are dependent on the specific instrumentation and methods used.[27] Therefore, our data were compared to the ratio of the reported elastic modulus of murine mammary cancer to that of the normal gland, with both measurements obtained using the same

Table 1. Elastic modulus measurements.

	Measured elastic modulus (Pa)	Reported elastic modulus (Pa)	Ratio of concentrations
1.9 mg/mL Collagen + 10% BM	84.1 ± 4.8		
6.0 mg/mL Collagen + 10% BM	1643.3 ± 200.2		19.5[a]
8.0 mg/mL Collagen + 10% BM	3433.3 ± 1201.6		40.8[b]
Normal mouse mammary gland[34]		167 ± 31	
Mouse mammary tumor[34]		4049 ± 938	24.2[c]

BM: basement membrane.
[a]6.0 mg/mL Collagen I + 10% BM divided by 1.9 mg/mL collagen I + 10% BM.
[b]8.0 mg/mL Collagen I + 10% BM divided by 1.9 mg/mL collagen I + 10% BM.
[c]Mouse mammary tumor divided by normal mouse mammary gland.

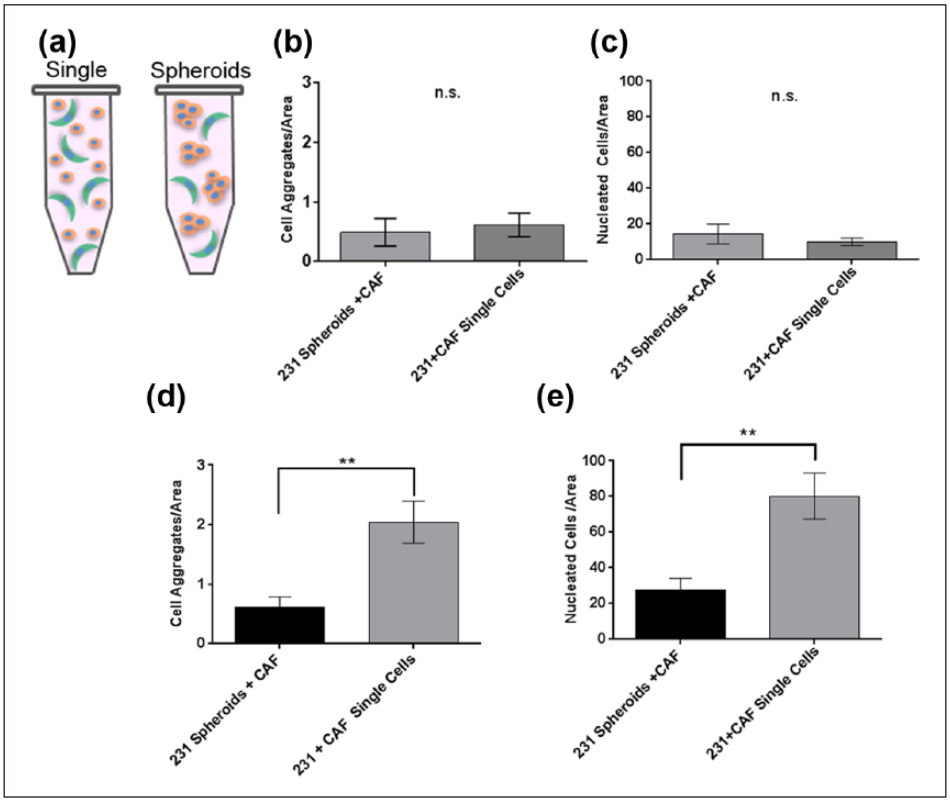

Figure 4. Optimization of method of cell incorporation. (a) Schematic of the two methods of cell incorporation—as single cells versus epithelial spheroids plus single CAF. Comparison of (b) aggregation and (c) cell density in solid surrogates with cells incorporated as preformed 231 cell spheroids with CAF or as single cells (both 231 and CAF) following 7 days growth (n = 4–6 surrogates per condition, unpaired t-test). Comparison of (d) aggregation and (e) cell density in perfused surrogates with cells incorporated as preformed 231 cell spheroids with CAF or as single cells (both 231 and CAF) after growth for 7 days (n = 6 surrogates per condition, unpaired t-test, **$p \leq 0.01$). Data in b–e are the mean and SEM.

method, which was a method similar to the one used by us.[33] The reported ratio of the elastic modulus of a murine mammary cancer to the corresponding normal mammary gland was 24.2 (4049–167 Pa).[33] Similarly for our data, the ratios of the elastic moduli of the ECM with 6.0 or 8.0 mg/mL collagen I to that with 1.9 mg/mL were 19.5 and 40.8, respectively. The elastic modulus of 2.0 mg/mL collagen gels has been reported to be similar to the elastic modulus of normal human breast.[29,34] The ratio derived using 6.0 mg/mL collagen more closely approximated the reported ratio of 24.2. In addition, 6.0 mg/mL allows for easier incorporation of cells than 8.0 mg/mL and was selected for subsequent use.

Method of cell incorporation into breast carcinoma surrogates

Next, the use of preformed spheroids of 231 cells, as opposed to single cells (depicted in Figure 4(a)), was examined as a potential means to promote EC aggregation.

Cell aggregation was compared after cells were incorporated into ECM (90% collagen I (6.0 mg/mL) and 10% BM) as either single cells (231 and CAF-hTERT, 2.1×10^6 total cells/100 µL ECM) or preformed spheroids of 231 cells with single CAF-hTERT (approximately 2.2×10^6 total cells/100 µL ECM). For preliminary analysis, 3D solid cultures (surrogates) in eight-well chamber slides were utilized with a starting E:F of 2:1 (median found in evaluation of histologic sections of human breast cancer). The surrogates were maintained in low-serum EC medium (DMEM + 0.05% FBS) for 7 days. Low-serum medium was selected to prevent masking of crosstalk between ECs and CAF. Following culture, surrogates were FFPE. Cell aggregation and density were assessed in complete, H&E-stained histologic cross sections of the surrogates, as described above. In the solid surrogates, there was no significant difference in aggregation (Figure 4(b)) or cell density (Figure 4(c)) between the methods of cell incorporation. To determine the relative performance in perfused surrogates, 231 spheroids plus single CAF-hTERT or single 231 and CAF-hTERT were incorporated into ECM as described for solid culture above, but prepared in the bioreactor and perfused for 7 days. Both aggregation (Figure 4(d)) and cell density (Figure 4(e)) were significantly increased in surrogates generated using single-cell incorporation compared to surrogates prepared using preformed epithelial spheroids (unpaired t-test, $p \leq 0.01$). Therefore, single cells were used to prepare surrogates moving forward.

Perfusion of surrogates enhanced growth at 7, 14, and 21 days culture

To evaluate the ability of our perfusion system to maintain surrogates in extended culture, surrogates with the same ECM (90% collagen I (6.0 mg/mL) and 10% BM) and cell (231 and CAF-hTERT (2:1), 2.1×10^6 total cells/100 µL ECM) composition (i.e. same initial cell seeding density) were prepared as 3D solid surrogates or as surrogates with 400 µm microchannels (prepared in the bioreactor flow channel) and either perfused (20 mL low-serum EC medium) or not perfused (non-perfused, that is, bioreactor flow channel placed in a medium bath (20 mL low-serum EC medium) after preparation). 3D solid surrogates were included in this comparison because this form of 3D culture is commonly utilized. Cell density and aggregation were measured in H&E-stained histologic sections of surrogates. At all time points, cell density was significantly greater in perfused surrogates than non-perfused or solid surrogates (Figure 5(a) and (b), one-way ANOVA with Sidak's multiple comparison testing, $p \leq 0.05$). At 7 days, cell density was also significantly higher in the non-perfused surrogates than in solid surrogates, but this was not sustained at 14 and 21 days. When looking at the same data over time (Figure 5(c)), perfused and non-perfused surrogates showed no significant change in cell density over the 2-week period (7–21 days), suggesting that much of the increase in cell number occurred during the first week of culture in surrogates with microchannels. However, cell density in solid surrogates increased over time (one-way ANOVA with Sidak's multiple comparison testing, $p \leq 0.05$), but there was a significant inverse correlation between this increase in cell density and the decrease in the total cross-sectional area of surrogates (i.e. the area measured) (Supplementary Figure 1, $p \leq 0.05$, Pearson's correlation coefficient, $r = -0.51$). There was a corresponding visible decrease in the overall sizes of solid surrogates during culture. Therefore, a possible explanation for the increased cell density in the solid surrogates over time is that the cells were compressed into a smaller area. Aggregation was greater in perfused surrogates compared to solid surrogates following 7 days of culture (Figure 5(d), one-way ANOVA with Sidak's multiple comparison testing, $p \leq 0.05$), but this difference did not persist over time. Given that the only difference between perfused and non-perfused surrogates is the presence of perfusion (identical size, composition, setup, amount of medium, and frequency of medium changes); perfusion is likely responsible for enhanced surrogate growth.

Proliferation was evaluated by Ki-67 labeling index in solid and perfused surrogates and found to be significantly increased in the perfused surrogates compared to solid surrogates at each time point (Figure 5(e), one-way ANOVA, $p \leq 0.001$). However, proliferation decreases in perfused surrogates between 14 and 21 days ($p \leq 0.05$ ANOVA), which may be a result of visible cell crowding on histologic sections in the perfused surrogates (appreciated in Figure 5(a)). There was no change over time in the percentage of cells which demonstrated immunohistochemical staining for cleaved caspase 3 in the perfused surrogates (Figure 5(f)), indicating no increase in apoptosis over time. In addition, less than 5% of cells are undergoing apoptosis at all time points evaluated. Together, these data support the use of our perfused surrogates for multi-week studies and indicate that our perfusion system better supports cell growth compared to traditional methods of 3D co-culture. However, at later time points, growth/proliferation is decreasing in this system using the culture parameters described.

Medium selection and cell seeding density affect growth and cell aggregation in perfused surrogates

To promote continued growth of the perfused surrogates, the medium formulation used and the initial number of cells seeded were optimized. Three different medium formulations were tested—(1) DMEM + 10% FBS (EC growth medium), (2) low-serum EC (0.05% FBS), and (3) mammary endothelial cell medium containing 5% FBS (HMMEC medium). Because of future plans to incorporate HMMECs into surrogates, growth curves of

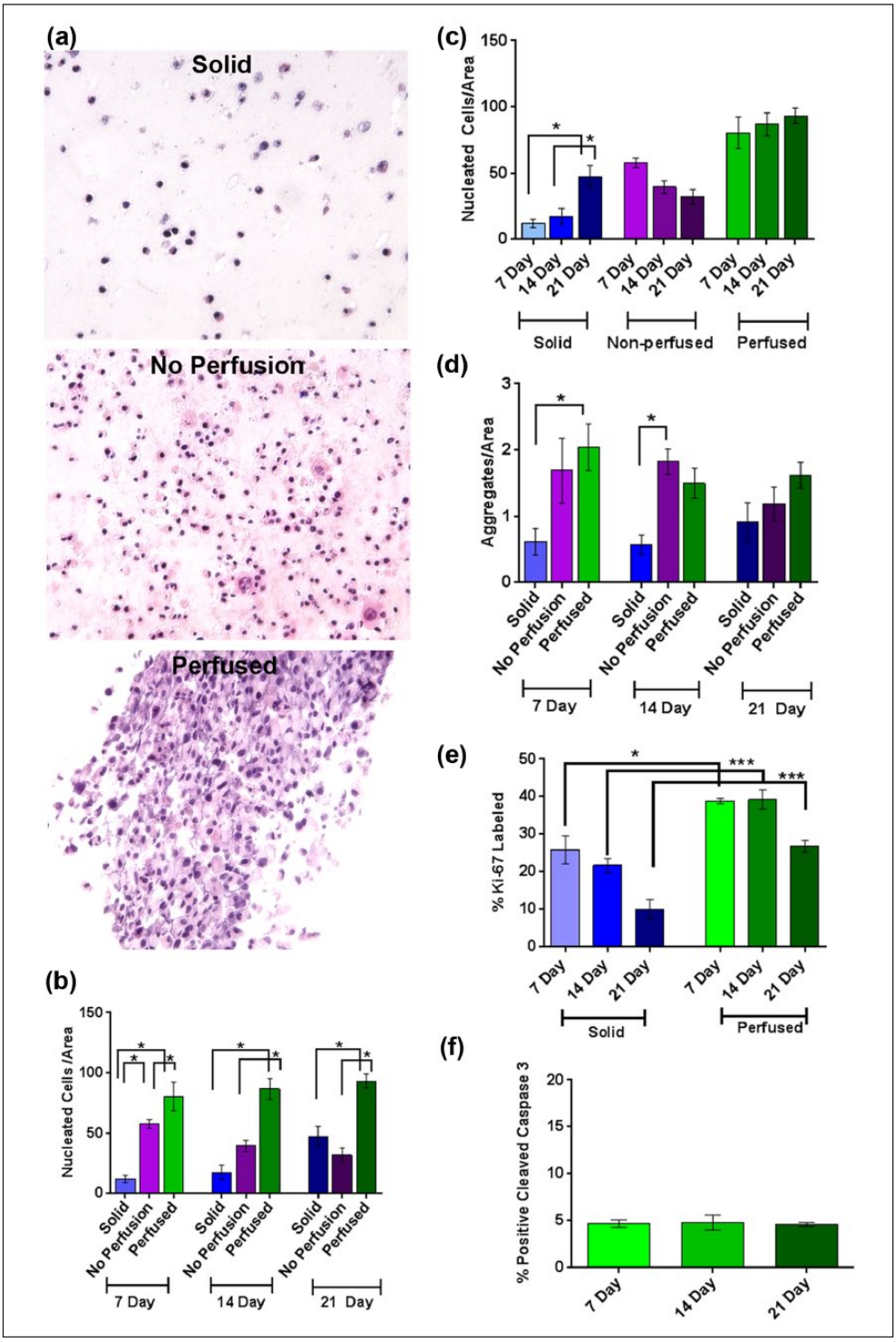

Figure 5. Culture of surrogates with and without perfusion for 7–21 days. (a) Representative photomicrographs of H&E-stained histologic sections from solid (top panel), non-perfused (middle panel), or perfused (bottom panel) surrogates cultured for 21 days (200× original magnification). (b, c) Cell density of perfused breast cancer surrogates compared to non-perfused and solid surrogates following 7, 14, and 21 days (n = 5–6 surrogates per condition and time point, one-way ANOVA with Sidak's multiple comparison testing, *p ⩽ 0.05). (d) Aggregation of perfused breast cancer surrogates compared to non-perfused and solid surrogates following 7, 14, and 21 days (n = 5–6 surrogates per condition and time point, one-way ANOVA with Sidak's multiple comparison testing, *p ⩽ 0.05). (e) Ki-67 labeling index in solid surrogates compared to perfused surrogates at 7, 14, and 21 days (n = 5–6 surrogates per condition and time point, one-way ANOVA with Sidak's multiple comparison testing, *p ⩽ 0.05 and ***p ⩽ 0.001). (f) Cleaved caspase 3 staining in the perfused surrogates at 7, 14, and 21 days (n = 3–5 surrogates at each time point, one-way ANOVA with Tukey's multiple comparison testing). Data in b–f are the mean and SEM.

231, CAF-hTERT, and HMMEC-hTERT in 2D culture were completed (Figure 6(a)) and showed that the HMMEC medium best supported the growth of all three cell lines. Next, HMMEC medium was compared to low-serum EC medium in perfused surrogates (ECM and cell composition as above) with a high cell seeding density (2.1×10^6 total cells/100 µL ECM, as above) or a low cell seeding density (1.05×10^6 total cells/100 µL ECM). After 21 days growth in low-serum EC medium, cell density and aggregation were significantly lower in the surrogates seeded at low density compared to those seeded at high density (Figure 6(b) and (c), unpaired t-tests, $p \leq 0.05$). However, in the HMMEC medium, initial seeding density had no impact on cell density and aggregation at 21 days. Furthermore, at the low seeding density, perfusion with HMMEC medium resulted in a higher cell density (borderline significance, $p = 0.05$) and significantly higher cell aggregation ($p \leq 0.05$) than the use of low-serum EC medium. These data indicate a growth promoting effect of HMMEC medium. However, seeding density had no impact on cell density or aggregation when HMMEC medium was used, suggesting that further growth and aggregation were curtailed after a maximum density was reached.

Some areas of the surrogates on histologic sections appeared to have higher cell density or crowding than others. The percent cross-sectional area of the surrogates occupied by cells after growth in the HMMEC medium for 21 days was assessed by image analysis of the histologic sections and was approximately 60% (Figure 6(e)). We theorized that continued growth might be limited by focal crowding. Therefore, in an attempt to better distribute the cells in the ECM during surrogate setup, and thereby allow more room for growth over time, rotation of surrogates during ECM polymerization was evaluated. Surrogates were seeded at the high seeding density with or without rotation during ECM polymerization and immediately fixed and processed. There was a significant increase in the area of ECM containing cells directly following ECM polymerization with the addition of surrogate rotation (Figure 6(d), unpaired t-test, $p \leq 0.05$). To evaluate whether surrogate rotation improved cell distribution after growth, surrogates were seeded at high and low seeding densities, rotated during ECM polymerization, and perfused with HMMEC medium for 21 days. The addition of rotation did not improve the distribution of cells at either low or high seeding density (Figure 6(e)). We hypothesize that this may be attributed to the use of the foam scaffold in our system. Although many of the foam pores are connected and continuous with one another, the foam may be hindering cell movement and expansion into unoccupied areas of the 3D volume. Based on these findings, cell seeding density will need to be modulated dependent on the experimental endpoint and cell types used, with longer growth periods requiring a lower cell seeding density to allow for growth over time.

The E:F ratio increases in perfused surrogates after multi-week growth

To determine whether the ratio of ECs (231) to fibroblasts (CAF-hTERT) (E:F) in perfused surrogates changes over time, the E:F was assessed by immunofluorescence (IF) staining for cell type–specific markers in surrogates perfused with HMMEC media for 7 and 21 days and seeded at high and low cell densities. IF was utilized because, unlike the cancer ECs and stromal fibroblasts in histologic sections of cancer tissues, the 231 and CAF-hTERT were not as consistent in morphology or location. The percentages of cells staining for CK8 (epithelial specific) and FAP (fibroblast specific) were counted on serial histologic sections of surrogates (Figure 7(a) and (b)). The initial seeding E:F was 2:1 (i.e. 67% 231 and 33% CAF-hTERT), as indicated by the horizontal lines in Figure 7(c) and (d). After 21 days at either seeding density, the percentages of 231 cells were greater than 67% (Figure 7(c)) and the percentages of CAF-hTERT were less than 33% (Figure 7(d)). This was also true for the CAF-hTERT at 7 days. After 21 days, there was an E:F of 5:1 at low seeding density and 3.5:1 at high seeding density. It is likely that the change in ratio can be attributed to a higher proliferation rate in the cancer ECs compared to the CAF, as we have observed in 2D cell culture (231 doubling rate: 16.2 h, CAF doubling rate: 40.3 h). However, the E:F remained within the range determined for human breast cancer (Figure 2).

Discussion

We have utilized a perfusion bioreactor system to develop a breast carcinoma tissue surrogate that has an overall volume of 1.2 cm^3 and can be maintained for at least 3 weeks. Nutrients and oxygen were delivered by continuously perfusing medium through microchannels (400 µm) which penetrate the 3D volume and function as a pseudo-vasculature, to sustain viability and promote growth throughout culture. The importance of the perfusion system to the growth and morphologic development of the surrogates was demonstrated by the greater cell density at all time points in the perfused surrogates compared to either solid or non-perfused surrogates. This system also enabled the added complexity associated with the tumor microenvironment that included human CAF and a relevant ECM. Because these surrogates included the 231 cell line, which is representative of the triple-negative subtype of breast carcinoma, they model triple-negative breast cancer. However, the cell components can be varied to model other subtypes of breast carcinoma or other cancer types, such as prostate or pancreatic cancer. In addition, the stromal cell types included could be tailored to address specific biological questions regarding the roles of specific components of the tumor microenvironment (e.g. the addition of adipocytes or tumor-associated macrophages).

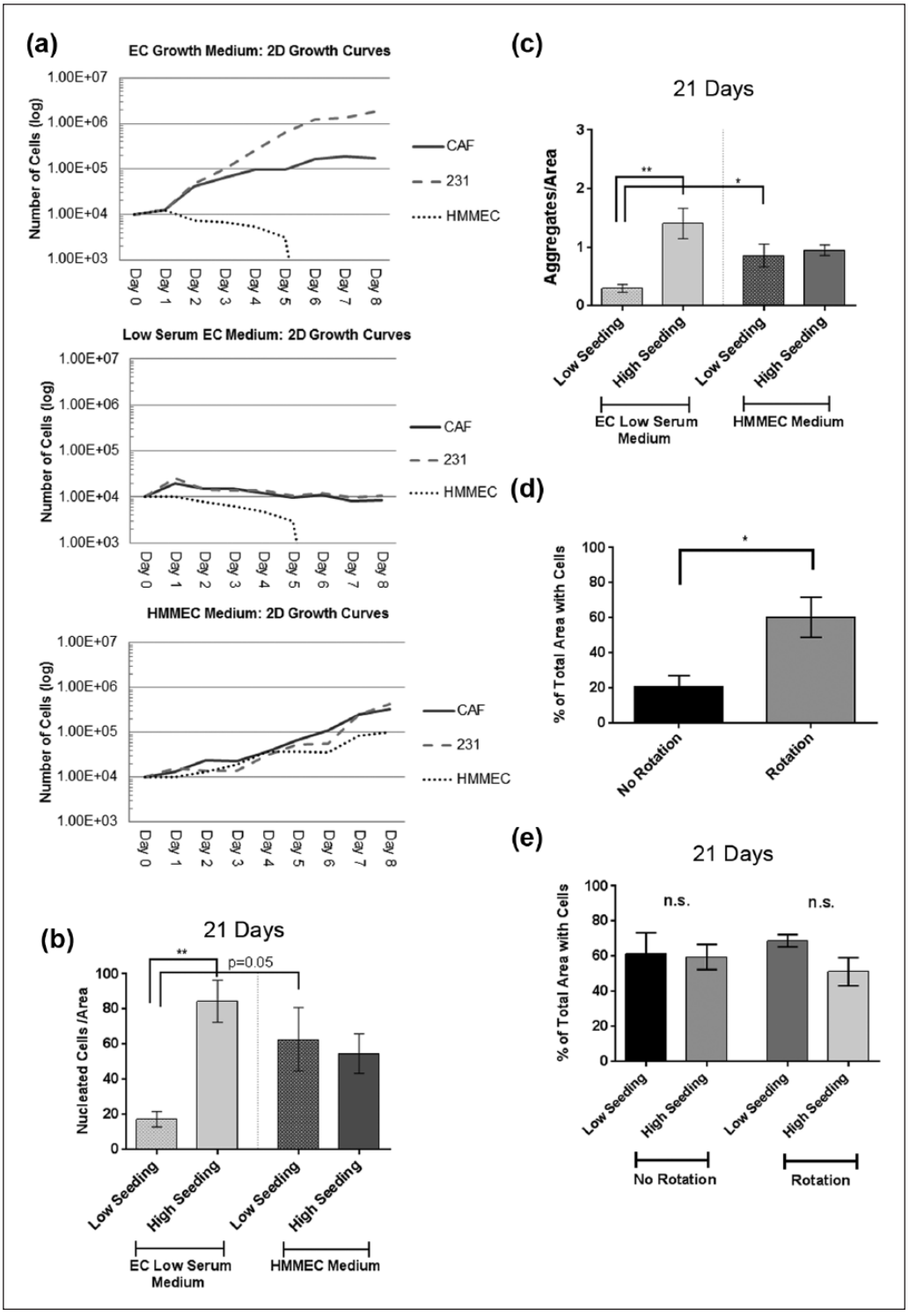

Figure 6. Evaluation of medium, cell seeding density, and cell distribution for long-term bioreactor culture. (a) Growth curves for CAF-hTERT, 231 cells, and HMMEC-hTERT when grown in EC medium (top panel), low-serum EC medium (middle panel), or HMMEC medium (bottom panel) in 2D culture. Data are the mean of three replicate wells for each time point. (b) Cell density and (c) cell aggregation in perfused surrogates at 21 days when initial cell seeding concentration was 2.1×10^6 cells/100 µL ECM (high) or 1.05×10^6 cells/100 µL ECM (low) and surrogates were cultured in low-serum EC (0.05% FBS) or HMMEC media (5% FBS) ($n = 4$–6 surrogates per condition, unpaired t-test, $^*p \leq 0.05$ and $^{**}p \leq 0.01$). (d) Evaluation of the effect of rotation during ECM polymerization on cell distribution immediately following ECM polymerization ($n = 5$ surrogates per condition, unpaired t-test, $^*p \leq 0.05$). (e) Cell distribution in perfused surrogates following perfusion for 21 days with HMMEC medium. The effect of rotation and cell seeding density (high versus low) were compared ($n = 4$ surrogates per condition, unpaired t-test). Data in b–e are the mean and SEM.

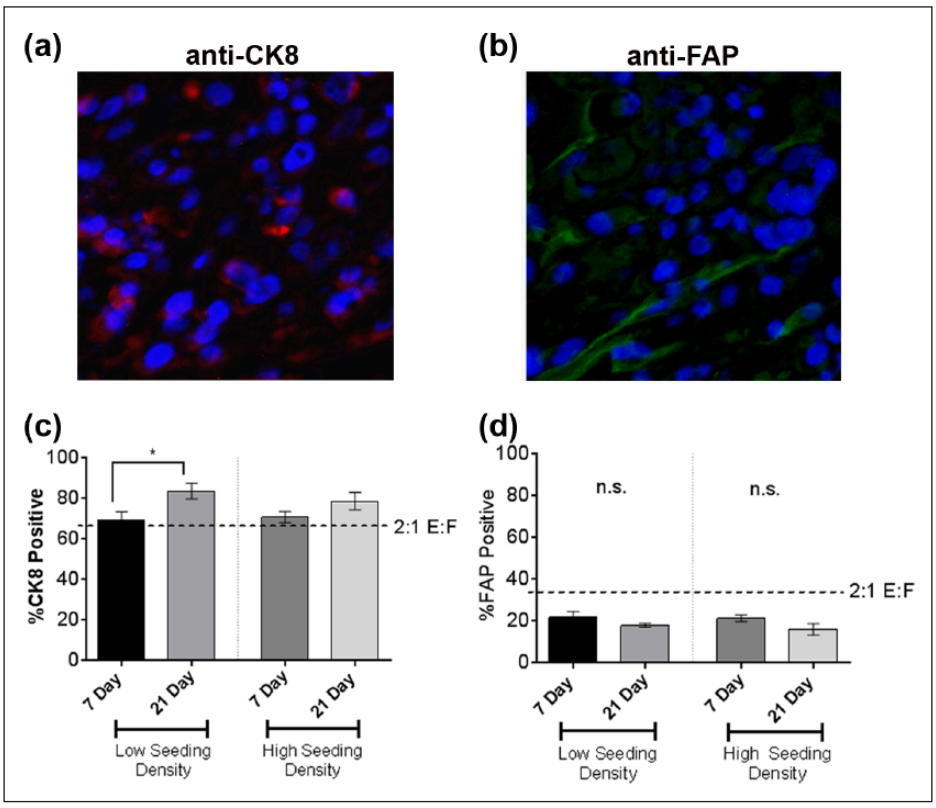

Figure 7. Epithelial to fibroblast ratio (E:F) following growth in the perfusion bioreactor system. (a) Representative photomicrograph of the CK8 immunofluorescence (IF) staining, marking epithelial cells with red fluorescence in the cytoplasm. Cells labeled red tend to cluster together, indicating epithelial cell aggregation. (b) Representative photomicrograph of the FAP IF staining, marking the cytoplasm of the CAF with green fluorescence (top panel). The green cytoplasm of the CAF in most cells is elongate, typical of fibroblast morphology. The CAF are interspersed among groups of non-labeled, clustering cells. (c) The percentage of CK8-positive cells following 7 or 21 days growth in the perfusion bioreactor system when surrogates were set up at low or high cell seeding densities (unpaired t-test,*$p \leq 0.05$). (d) The percentage of FAP-positive cells following 7 or 21 days growth in the perfusion bioreactor system when surrogates were set up at low or high cell seeding densities ($n = 4$ surrogates at each time point and seeding density in c and d). Data in c and d are the mean and SEM.

The ability to maintain the surrogates for multiple weeks permits time for recapitulative morphologic development and potentially for the development of recapitulative tissue biomechanics. The longer culture duration also allows for evaluation of cell–cell and cell–ECM interactions over time. The greater dimensionality and growth period may better predict the efficacy of candidate therapeutics, including the development of drug resistance, which will require extended culture for evaluation.

Triple-negative breast cancers are typically high-grade carcinomas, with a high rate of proliferation and a relatively low degree of cell aggregation.[35,36] Therefore, the morphology of the surrogates described here should resemble high-grade (i.e. grade 3) breast carcinomas. Indeed, the overall histologic morphology of the perfused surrogates (Figure 5(a), bottom panel) resembles some of the high-grade breast carcinomas that we evaluated, such as case 6 in Figure 2, in which there are sheets of crowded malignant ECs with minimal intervening stroma. In addition, the mean of each of the measured parameters—E:F, cell aggregation, cell density (5:1, 0.86 aggregates per area and 62.8 cells per area, respectively)—of the surrogates grown for 21 days in HMMEC medium using the low seeding density fell within the range of values obtained from the human breast carcinomas, most of which were grade 3 (Figure 2). The cell density of the surrogates, however, was at the higher end of the range for the breast cancer specimens, which may result from the limited room for expansion imposed by the presence of the PDMS foam or a relatively high initial seeding density. While some areas of necrosis were identified in multi-week surrogates, this is representative of breast carcinoma in patients, which often contain areas of necrosis as well as areas of actively proliferating cells.[36–38]

Media composition and the initial cell seeding density affected growth and morphologic development and require consideration during the development of model systems, such as the one described. We found that the use of preformed epithelial spheroids and rotating the tissue surrogates during ECM polymerization were not helpful in promoting surrogate growth or morphologic recapitulation. Single-cell incorporation of ECs and CAF was found to better promote cell density/growth and aggregation, compared

to the use of preformed epithelial spheroids in perfused surrogates. While surrogate rotation did help to better distribute cells prior to growth, this affect was lost over time.

In the future, HMMECs will be incorporated into our breast cancer surrogates (lining the microchannels) to further recapitulate the microenvironment, and microvasculature, present in vivo. This addition will add another layer of complexity to our system, one which may be critical for the evaluation of delivery and efficacy of certain therapeutics.[39] An updated bioreactor design that does not require the use of a foam backbone or contains foam with a larger pore size may be beneficial moving forward in order to better distribute cells throughout the 3D volume. In turn, a lower cell seeding density and more even cell distribution may aid in better recapitulation of tissue architecture and make longer growth periods possible, without hindering viability. This will be particularly important for extended evaluation of therapeutic efficacy and recurrence/development of resistance. Additionally, PDMS is known to absorb hydrophobic molecules, including therapeutics, which could impact the testing of therapeutic efficacy.[40–43] Therefore, the use of other flexible, inert, and clear materials, such as polyurethane, will be considered prior to utilization of this system for drug testing.[44]

Since larger 3D models, similar to the one described here, are not widely used at this time, many analytical methods developed for 2D cell culture, including viability assays, have not yet been adapted for use in 3D tissue models, particularly larger models such as ours.[45] Increased dimensionality can hinder traditional imaging-based methods of analysis; therefore, many quantifiable measurements may need to be completed as terminal endpoints resulting in dissolution or processing of the 3D culture. Here, tissue processing and histologic analysis was the terminal analytic method used and provided optimal morphologic analysis for comparison to human breast carcinomas. Moving forward, additional terminal analyses, such as molecular analysis of specific cell populations, or non-destructive analyses, such as interim analysis of perfusates or real-time imaging of surrogates, will be developed to provide additional information about the cellular and molecular response to therapy or other stimuli.

The utility of multi-cellular 3D models for in vitro investigation of the interplay between malignant cells and the stromal microenvironment as well as how this cross-talk influences drug response has been increasingly appreciated and utilized in the field of cancer biology.[46] Recently, complex 3D systems have been utilized to model different stages and processes in breast cancer including the pathogenesis of breast cancer from the ductal carcinoma in situ stage,[47,48] common sites of breast cancer metastatic dissemination (e.g. bone[49,50] and liver[51]), and the interactions between breast cancer cells and immune cell populations.[52] These models were used to evaluate specific biological processes driving breast cancer development, metastasis, dormancy, and immune modulation. These systems often utilized a microfluidic platform or solid 3D cultures and differed from our surrogate system by being smaller in size, having a different method of perfusion (or no perfusion) and different cell–ECM composition. Our breast carcinoma surrogate system has been developed as a model of primary breast cancer, at a size in which a human tumor could be detected by mammography, and cultured for multiple weeks to allow for development of tumor architecture. The larger size and ECM component of our surrogates also distinguishes them from 3D culture systems currently utilized for preclinical drug testing, which often consist of multi-cellular spheroids.[53–55] Moving forward, the utility of this system will be evaluated for preclinical testing of new therapeutics.

Conclusion

The 3D in vitro breast carcinoma tissue surrogates described here include a tumor microenvironment consisting of ECM and human CAF and have a dimensionality that approximates breast cancer size at diagnosis. Growth and maintenance of these surrogates for 21 days required the use of a perfusion system to provide necessary oxygen and nutrients. Complex 3D systems such as these require fine tuning of each component to provide the optimal growth environment for morphologic development, extended culture, and subsequent analysis. This model system has the potential for various applications in the evaluation of molecular processes driving carcinogenesis and cancer progression, evaluation of the efficacy of candidate therapeutics, and cancer resistance and recurrence after initiation of therapy.

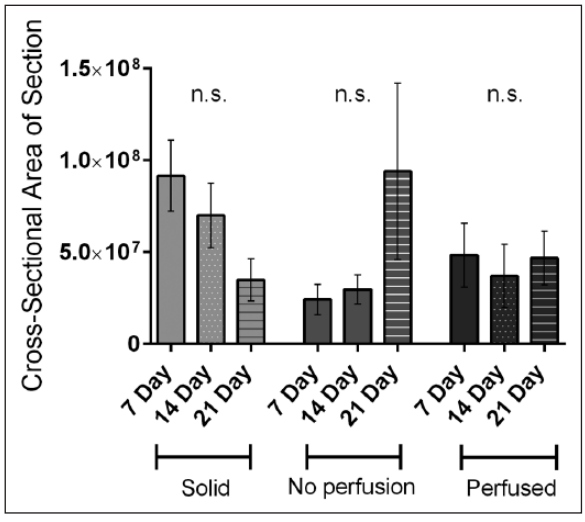

Supplemental Figure 1. Changes in average cross-sectional area. The average area of the complete histological cross-section of solid, non-perfused, and perfused surrogates following 7, 14, and 21 days culture was measured (n = 5–6 surrogates per experimental condition, one-way ANOVA with Sidak's multiple comparison testing).

Acknowledgements

The authors would like to thank Tim Fee and Didarul Bhuiyah for technical assistance with compression testing and the UAB Pathology Core Research Lab for assistance in the processing, sectioning, and H&E staining of surrogates. They gratefully acknowledge bioreactor manufacturing assistance from Southern Research, Birmingham, AL.

Declaration of conflicting interests

The author(s) declared no potential conflicts of interest with respect to the research, authorship, and/or publication of this article.

Funding

The author(s) disclosed receipt of the following financial support for the research, authorship, and/or publication of this article: This work was supported by the United States Department of Defense Breast Cancer Research Program (BC121367).

References

1. Olson P, Chu GC, Perry SR, et al. Imaging guided trials of the angiogenesis inhibitor sunitinib in mouse models predict efficacy in pancreatic neuroendocrine but not ductal carcinoma. *Proc Natl Acad Sci U S A* 2011; 108: 19455–19456.
2. Hakanson M, Textor M and Charnley M. Engineered 3D environments to elucidate the effect of environmental parameters on drug response in cancer. *Integr Biol* 2011; 3: 31–38.
3. Elliott NT and Yuan F. A review of three-dimensional in vitro tissue models for drug discovery and transport studies. *J Pharm Sci* 2011; 100: 59–74.
4. Gibbons MC, Foley MA and Cardinal KO. Thinking inside the box: keeping tissue-engineered constructs in vitro for use as preclinical models. *Tissue Eng Part B Rev* 2013; 19: 14–30.
5. Weigelt B, Ghajar CM and Bissell MJ. The need for complex 3D culture models to unravel novel pathways and identify accurate biomarkers in breast cancer. *Adv Drug Deliv Rev* 2014; 69–70: 42–51.
6. Lovitt CJ, Shelper TB and Avery VM. Advanced cell culture techniques for cancer drug discovery. *Biology* 2014; 3: 345–367.
7. Park JH, Chung BG, Lee WG, et al. Microporous cell-laden hydrogels for engineered tissue constructs. *Biotechnol Bioeng* 2010; 106: 138–148.
8. Correa de Sampaio P, Auslaender D, Krubasik D, et al. A heterogeneous in vitro three dimensional model of tumour-stroma interactions regulating sprouting angiogenesis. *PLoS One* 2012; 7: e30753.
9. Salameh TS, Le TT, Nichols MB, et al. An ex vivo co-culture model system to evaluate stromal-epithelial interactions in breast cancer. *Int J Cancer* 2013; 132: 288–296.
10. Shekhar MP, Santner S, Carolin KA, et al. Direct involvement of breast tumor fibroblasts in the modulation of tamoxifen sensitivity. *Am J Pathol* 2007; 170: 1546–1560.
11. Li L and Lu Y. Optimizing a 3D culture system to study the interaction between epithelial breast cancer and its surrounding fibroblasts. *J Cancer* 2011; 2: 458–466.
12. Hay M, Thomas DW, Craighead JL, et al. Clinical development success rates for investigational drugs. *Nat Biotechnol* 2014; 32: 40–51.
13. Sonnenberg M, Van der Kuip H, Haubeis S, et al. Highly variable response to cytotoxic chemotherapy in carcinoma-associated fibroblasts (CAFs) from lung and breast. *BMC Cancer* 2008; 8: 364.
14. Kim JB, Stein R and O'Hare MJ. Three-dimensional in vitro tissue culture models of breast cancer: a review. *Breast Cancer Res Treat* 2004; 85: 281–291.
15. Weiswald LB, Bellet D and Dangles-Marie V. Spherical cancer models in tumor biology. *Neoplasia* 2015; 17: 1–15.
16. Michaelson J, Satija S, Moore R, et al. Estimates of the sizes at which breast cancers become detectable on mammographic and clinical grounds. *J Women's Imaging* 2003; 5: 3–10.
17. Cassereau L, Miroshnikova YA, Ou G, et al. A 3D tension bioreactor platform to study the interplay between ECM stiffness and tumor phenotype. *J Biotechnol* 2015; 193: 66–69.
18. Marshall LE, Goliwas KF, Miller LM, et al. Flow-perfusion bioreactor system for engineered breast cancer surrogates to be used in preclinical testing. *J Tissue Eng Regen Med*. Epub ahead of print 7 May 2015. DOI: 10.1002/term.2026.
19. Galea MH, Blamey RW, Elston CE, et al. The Nottingham Prognostic Index in primary breast cancer. *Breast Cancer Res Treat* 1992; 22: 207–219.
20. Sadlonova A, Novak Z, Johnson MR, et al. Breast fibroblasts modulate epithelial cell proliferation in three-dimensional in vitro co-culture. *Breast Cancer Res* 2005; 7: R46–R59.
21. Calcagnile P, Fragouli D, Mele E, et al. Polymeric foams with functional nanocomposite cells. *RSC Adv* 2014; 4: 1977–19182.
22. Bergamaschi A, Tagliabue E, Sørlie T, et al. Extracellular matrix signature identifies breast cancer subgroups with different clinical outcome. *J Pathol* 2008; 214: 357–367.
23. Oskarsson T. Extracellular matrix components in breast cancer progression and metastasis. *Breast* 2013; 22: S66–S72.
24. Naba A, Clauser KR, Lamar JM, et al. Extracellular matrix signatures of human mammary carcinoma identify novel metastasis promoters. *eLife* 2014; 3: e01308.
25. Kelley LC, Lohmer LL, Hagedorn EJ, et al. Traversing the basement membrane in vivo: a diversity of strategies. *J Cell Biol* 2014; 204: 291–301.
26. Wolf K, Alexander S, Schacht V, et al. Collagen-based cell migration models in vitro and in vivo. *Semin Cell Dev Biol* 2009; 20: 931–941.
27. Schedin P and Keely PJ. Mammary gland ECM remodeling, stiffness, and mechanosignaling in normal development and tumor progression. *Cold Spring Harb Perspect Biol* 2011; 3: a003228.
28. Cox TR and Erler JT. Remodeling and homeostasis of the extracellular matrix: implications for fibrotic diseases and cancer. *Dis Model Mech* 2011; 4: 165–178.
29. Wellman PS, Howe RD, Dalton E, et al. Breast tissue stiffness in compression is correlated to histological diagnosis. *Technical Report. Harvard BioRobotics Laboratory* 1999; 1–15.

30. Levental KR, Yu H, Kass L, et al. Matrix crosslinking forces tumor progression by enhancing integrin signaling. *Cell* 2009; 139: 891–906.
31. Provenzano PP, Inman DR, Eliceiri KW, et al. Matrix density-induced mechanoregulation of breast cell phenotype, signaling and gene expression through a FAK-ERK linkage. *Oncogene* 2009; 28: 4326–4343.
32. Chaudhuri O, Koshy ST, Branco da Cunha C, et al. Extracellular matrix stiffness and composition jointly regulate the induction of malignant phenotypes in mammary epithelium. *Nat Mater* 2014; 13: 970–978.
33. Wolf K, Te Lindert M, Krause M, et al. Physical limits of cell migration: control by ECM space and nuclear deformation and tuning by proteolysis and traction force. *J Cell Biol* 2013; 201: 1069–1084.
34. Paszek MJ, Zahir N, Johnson KR, et al. Tensional homeostasis and the malignant phenotype. *Cancer Cell* 2005; 8: 241–254.
35. Reis-Filho JS and Tutt AN. Triple negative tumours: a critical review. *Histopathology* 2008; 52: 108–118.
36. Schmadeka R, Harmon BE and Singh M. Triple-negative breast carcinoma: current and emerging concepts. *Am J Clin Pathol* 2014; 141: 462–477.
37. Rakha EA, Reis-Filho JS and Ellis IO. Basal-like breast cancer: a critical review. *J Clin Oncol* 2008; 26: 2568–2581.
38. Corben AD. Pathology of invasive breast disease. *Surg Clin North Am* 2013; 93: 363–392.
39. Jain RK. Normalization of tumor vasculature: an emerging concept in antiangiogenic therapy. *Science* 2005; 307: 58–62.
40. Halldorsson S, Lucumi E, Gomez-Sjoberg R, et al. Advantages and challenges of microfluidic cell culture in polydimethylsiloxane devices. *Biosens Bioelectron* 2015; 63: 218–231.
41. Regehr KJ, Domenech M, Koepsel JT, et al. Biological implications of polydimethylsiloxane-based microfluidic cell culture. *Lab Chip* 2009; 9: 2132–2139.
42. Toepke MW and Beebe DJ. PDMS absorption of small molecules and consequences in microfluidic applications. *Lab Chip* 2006; 6: 1484–1486.
43. Wang JD, Douville NJ, Takayama S, et al. Quantitative analysis of molecular absorption into PDMS microfluidic channels. *Ann Biomed Eng* 2012; 40: 1862–1873.
44. Domansky K, Leslie DC, McKinney J, et al. Clear castable polyurethane elastomer for fabrication of microfluidic devices. *Lab Chip* 2013; 13: 3956–3964.
45. Antoni D, Burckel H, Josset E, et al. Three-dimensional cell culture: a breakthrough in vivo. *Int J Mol Sci* 2015; 16: 5517–5527.
46. Stadler M, Walter S, Walzl A, et al. Increased complexity in carcinomas: analyzing and modeling the interaction of human cancer cells with their microenvironment. *Semin Cancer Biol* 2015; 35: 107–124.
47. Choi Y, Hyun E, Seo J, et al. A microengineered pathophysiological model of early-stage breast cancer. *Lab Chip* 2015; 15: 3350–3357.
48. Bischel LL, Beebe DJ and Sung KE. Microfluidic model of ductal carcinoma in situ with 3D, organotypic structure. *BMC Cancer* 2015; 15: 12.
49. Marlow R and Dontu G. Modeling the breast cancer bone metastatic niche in complex three-dimensional cocultures. *Methods Mol Biol* 2015; 1293: 213–220.
50. Subia B, Dey T, Sharma S, et al. Target specific delivery of anticancer drug in silk fibroin based 3D distribution model of bone-breast cancer cells. *ACS Appl Mater Interfaces* 2015; 7: 2269–2279.
51. Wheeler SE, Clark AM, Taylor DP, et al. Spontaneous dormancy of metastatic breast cancer cells in an all human liver microphysiologic system. *Br J Cancer* 2014; 111: 2342–2350.
52. Augustine TN, Dix-Peek T, Duarte R, et al. Establishment of a heterotypic 3D culture system to evaluate the interaction of TREG lymphocytes and NK cells with breast cancer. *J Immunol Methods* 2015; 426: 1–13.
53. Taubenberger AV, Bray LJ, Haller B, et al. 3D extracellular matrix interactions modulate tumour cell growth, invasion and angiogenesis in engineered tumour microenvironments. *Acta Biomater* 2016; 36: 73–85.
54. Sabhachandani P, Motwani V, Cohen N, et al. Generation and functional assessment of 3D multicellular spheroids in droplet based microfluidics platform. *Lab Chip* 2016; 16: 497–505.
55. Sethi P, Jyoti A, Swindell EP, et al. 3D tumor tissue analogs and their orthotopic implants for understanding tumor-targeting of microenvironment-responsive nanosized chemotherapy and radiation. *Nanomedicine* 2015; 11: 2013–2023.